



Politecnico di Torino

## Porto Institutional Repository

[Article] Mixing of a passive scalar across a thin shearless layer:  
Concentration of intermittency on the sides of the turbulent interface

*Original Citation:*

M. Iovieno; S. Di Savino; L. Gallana; D. Tordella (2014). *Mixing of a passive scalar across a thin shearless layer: Concentration of intermittency on the sides of the turbulent interface*. In: [JOURNAL OF TURBULENCE](#), vol. 15 n. 5, pp. 311-334. - ISSN 1468-5248

*Availability:*

This version is available at : <http://porto.polito.it/2543316/> since: May 2014

*Publisher:*

Taylor & Francis

*Published version:*

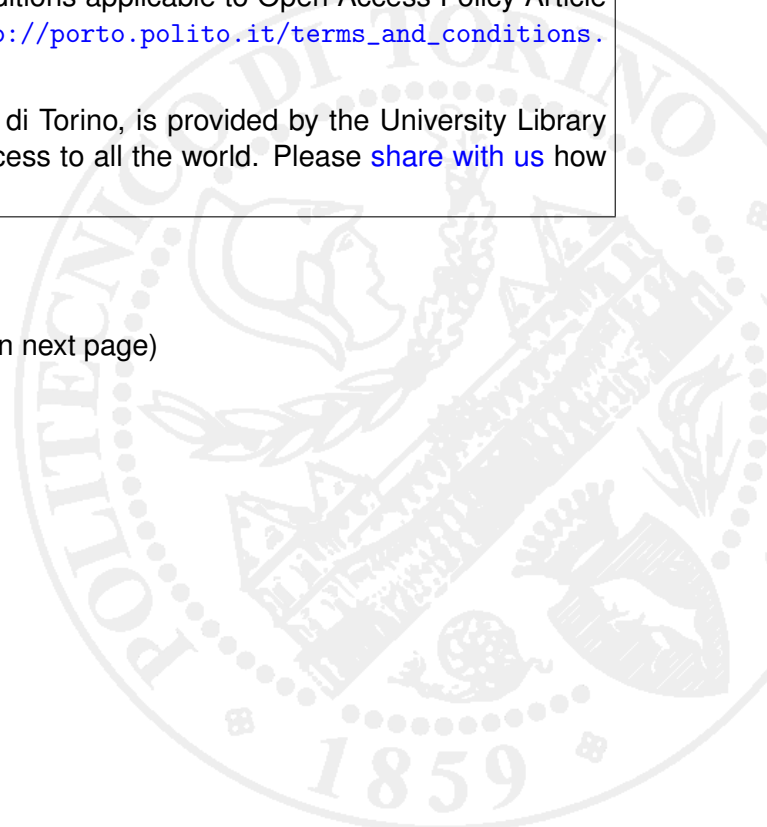
DOI:[10.1080/14685248.2014.905393](https://doi.org/10.1080/14685248.2014.905393)

*Terms of use:*

This article is made available under terms and conditions applicable to Open Access Policy Article ("Public - All rights reserved") , as described at [http://porto.polito.it/terms\\_and\\_conditions.html](http://porto.polito.it/terms_and_conditions.html)

Porto, the institutional repository of the Politecnico di Torino, is provided by the University Library and the IT-Services. The aim is to enable open access to all the world. Please [share with us](#) how this access benefits you. Your story matters.

(Article begins on next page)



Coll: KD QA: TA

*Journal of Turbulence*, 2014  
 Vol. 0, No. 0, 1–24, <http://dx.doi.org/10.1080/14685248.2014.905393>



## Mixing of a passive scalar across a thin shearless layer: concentration of intermittency on the sides of the turbulent interface

M. Iovieno, S. Di Savino, L. Gallana and D. Tordella\*

*Dipartimento di Ingegneria Meccanica e Aerospaziale, Politecnico di Torino, Torino, Italy*

5 (Received 6 December 2013; accepted 12 March 2014)

The advection of a passive scalar through an initial flat interface separating two different isotropic decaying turbulent fields is investigated in two and three dimensions. Simulations have been performed for a range of Taylor's microscale Reynolds numbers from 45 to 250 and for a Schmidt number equal to 1. Different to the case where the transport involves the momentum and kinetic energy only and one intermittency layer is formed in the low-turbulent energy side of the system, in the passive scalar concentration field two intermittent layers are observed to develop at the sides of the interface. The layers move normally to the interface in opposite directions. The dimensionality produces different time scaling of the passive scalar diffusion, which is much faster in the two-dimensional case. In two dimensions, the propagation of the intermittent layers exhibits a significant asymmetry with respect to the initial position of the interface and is deeper for the layer which moves towards the high kinetic energy side of the system. In three dimensions, the two intermittent layers propagate nearly symmetrically with respect the centre of the mixing region. During the temporal decay, inside the mixing, which is both inhomogeneous and anisotropic but devoid of a mean velocity shear, the passive scalar spectra are computed. In three dimensions, the exponent in the scaling range gets in time a value close to that of the kinetic energy spectrum of isotropic turbulence ( $-5/3$ ). In two dimensions, instead the exponent settles down to a value that is about one-half of the corresponding isotropic case. By means of an analysis based on simple wavy perturbations of the interface we show that the formation of the double layer of intermittency is a dynamic general feature not specific to the turbulent transport. These results of our numerical study are discussed in the context of experimental results and numerical simulations.

30 **Keywords:** turbulent transport; passive scalar; shearless mixing; intermittency; spectral scaling

### 1. Introduction

A passive scalar is a contaminant in a fluid flow that has no dynamical effects on the fluid motion itself. The transport of a passive substance within a turbulent velocity field is an important process in many natural and engineering contexts, like chemical mixing, combustion, and pollutant dispersal in oceanography and atmospheric science. In all these situations, the prediction of mixing and dispersion rates of a scalar contaminant is of great interest because of the concern over the efficiency of mixing and combustion and environmental pollution. Moreover, the propagation of light and radio waves in the atmosphere is

\*Corresponding author. Email: [daniela.tordella@polito.it](mailto:daniela.tordella@polito.it)

Q1

Q2

35

also influenced by the distribution of small-scale temperature gradients and water vapour concentration, which almost behave like a passively advected substance.

The lines of constant scalar concentration undergo stretching and folding in a spatially non-uniform flow velocity field. This leads to a progressive increase in the local gradients of the scalar field which is blocked ultimately by the smoothing action of molecular diffusion. Although the concentration of a passive substance exhibits a complex behaviour that shows some phenomenological parallels with the behaviour of the advecting turbulent velocity field, the statistical properties of passive scalar concentration are only partly influenced by the Kolmogorov cascade phenomenology. The phenomenological picture of scalar transport is thus undergoing a reinterpretation in last years as empirical evidence shows that local isotropy, both at the inertial and dissipation scales, is violated (see the recent reviews by Sreenivasan and Antonia [1], Shraiman and Siggia [2], and Warhaft [3]).

The classical view due to Taylor–Kolmogorov of small-scale velocity and scalar fields in fully developed turbulence was that the small scales are not directly advected by large-scale conditions, and therefore, must be locally isotropic. This view does not agree with the measurements of higher moments in turbulent flows with anisotropic or intermittent large-scale motions or anisotropic forcing [2,4,5]. In the case of an imposed mean scalar gradient, experimental measurements and numerical simulations show that the gradients aligned with the imposed mean gradient are on average larger than those perpendicular to the mean gradient [3,6,7]. The data do not indicate that the small scales tend to become isotropic as the Reynolds number increases.

Recent progress in the statistical description of passive scalar turbulence centred on the realisation that anomalous scaling properties and the appearance of coherent structures in the scalar field – well-known characteristics of fluid turbulence itself – occur even for a scalar advected by a simple random Gaussian velocity field [8–10].

Moreover, dispersion usually occurs in time-dependent inhomogeneous flows, which present a much more complicate behaviour than homogeneous flows, and thus are beyond the reach of analytical models or, in many cases, even numerical simulations. A simple inhomogeneous time-dependent situation that can be numerically analysed is a shear-free mixing layer. The mixing, for this case, is an important test field for the non-trivial statistical aspects of the scalar which the studies show [2,11,12] to originate in the mixing process itself, rather than being inherited from the complexity of the turbulent velocity field.

In this paper, we study the turbulent transport of a passive scalar across an interface which is represented by a mean scalar gradient. The interface matches two isotropic turbulent fields with different levels of kinetic energy. A local turbulent energy gradient is thus associated with the scalar one. The field that transports it is formed by one high kinetic energy turbulent isotropic field which is left to convectively diffuse into a lower energy one. In this shear-free velocity field, the region where the two turbulences interact is preceded by a highly intermittent thin layer – where the energy flux is maximum – that propagates into the low-energy region (see [13–16]). It should be noticed that this particular fluctuation field features a compression of the fluid filaments normal to the interface, that is along the direction of the mean gradient of both the scalar and kinetic energy fields. This is accompanied by the stretching of the fluid filaments parallel to the interface and is signature of the small-scale anisotropy [15]. It should be noticed that local compression in the straining motion is also a feature associated with the ramp and cliff structure of the scalar field observed in the case of an imposed mean scalar gradient in anisotropic turbulent-like flow field [3,10,17].

Our system is actually an initial-value problem where the initial step of turbulent energy and passive scalar is observed to evolve. The study is carried out with the help of the direct numerical simulation of the Navier–Stokes and advective–diffusive equations.

This study highlights two aspects of the mixing process. First, we show that there is a significant difference in terms of structure and intensity of the intermittency between the scalar field and the velocity field which transports the scalar. Second, we contrast mixing in our flow with the scalar mixing in simpler, homogeneous, turbulent flows. 90

In particular, we highlight the formation of a double intermittent layer bounding the interface between the regions where the passive scalar field is present and those in which it is not here yet. This aspect has not been evidenced in the previous literature, though it can be surely observed in the experiment by Ma and Warhaft [18] ( $Re_\lambda \sim 33$ ), where the focus was on the self-similarity of the temperature moments as a function of the method used to generate a temperature step in homogeneous grid turbulence and on the comparison of flux coefficients with linear gradient experiments. In another laboratory experiment by Jayesh and Warhaft [19], the evolution of a stably stratified interface, with strong turbulence below and quiescent air above, was studied. Though the physics is different because of the density stratification, by observing Figures 16 and 17 therein, which contain third-order mixed moments at rather low Richardson numbers, one can see that the distributions show a similar trend to those presented in this study (cf. Figures 7 and 8 below). 95 100

Anyway, the double intermittent layer should also be present at the interfaces bounding free flows even if it is hard to detect such a feature in fields where complex non-flat interfaces are present, as in the jet and wake cases. In fact, in studies where the interface detection was successfully carried out, for example, the experiment by Westerweel *et al.* [20] on submerged water jets, the focus was put on the boundary entrainment quantification and on discontinuities in the mean axial velocity and mean scalar and on singularity in the mean vorticity at the interface. We think that a posteriori second analysis of the Westerweel *et al.* data [20] can show the existence of a double intermittent layer. 105 110

The initial condition construction and computational method are described in Section 2. In Section 3, we document the passive scalar turbulent transport in two and three dimensions by means of one-point Eulerian statistics, which describe the first four moments of the passive scalar concentration, the skewness, and kurtosis of the passive scalar derivative and the passive scalar spectra. We compare the transport in two-dimensional (2D) and three-dimensional (3D) turbulence. The integral scale Reynolds number is about 3000 in both cases, which corresponds to a Taylor microscale Reynolds number  $Re_\lambda$  up to 250. In Section 3.3, we show that the double intermittency layer can be generated by simple transverse wave perturbations of the initial interface separating the velocity and passive scalar fields. The summary is in Section 4. 115 120

## 2. Method

The Navier–Stokes equations for an incompressible fluid have been solved in a parallelepiped domain together with the advection–diffusion equation for a passive scalar:

$$\frac{\partial \theta}{\partial t} + u_j \frac{\partial \theta}{\partial x_j} = \kappa \nabla^2 \theta, \quad (1)$$

where  $\theta$  is the passive scalar concentration,  $u_j$  is the velocity field, and  $\kappa$  is the diffusivity of the passive scalar. Figure 1 shows a schematic diagram of the flow configuration and the coordinate system used. For the initial condition, two isotropic fields are separated by a thin layer which is as thick as the correlation length  $\ell$ . From a numerical point of view, the flow is assumed to be contained in a parallelepiped (or a rectangle in two dimensions) and periodic boundary conditions are applied to all the spatial directions. The coordinate 125 130

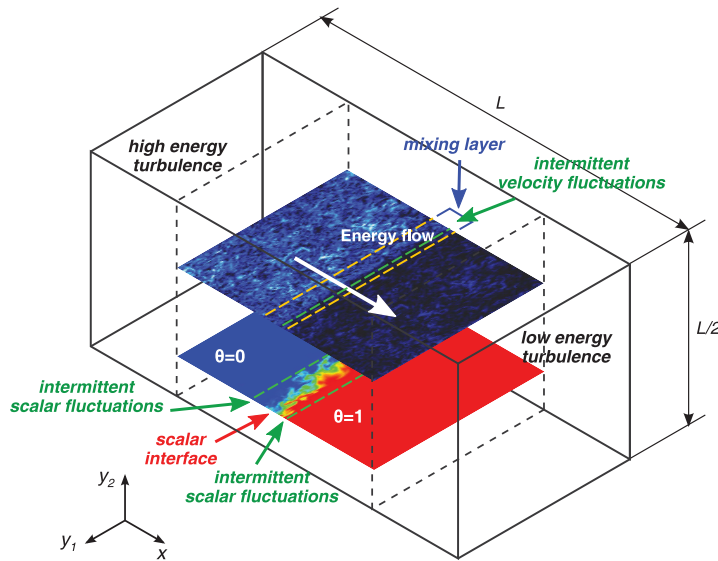


Figure 1. Scheme of the flow showing the coordinate system and the flow configuration. Due to the use of periodic boundary conditions, two mixing layers are included in the computational domain along the  $x$ -direction, which is the direction where the inhomogeneity takes places. The dashed lines indicate the central part of the domain where results are presented. The flow is homogeneous in the other two directions  $y_1$  and  $y_2$ .  $L$  is the domain size in  $x$ -direction, equal to  $4\pi$  in dimensional form. As a reference dimensional field, we considered the following set of data: domain size  $L = 4.1$  m, kinematic viscosity  $1.5 \times 10^{-5}$  m<sup>2</sup>/s, integral scale  $\ell = 1.0 \times 10^{-1}$  m and turbulent kinetic energy  $E_1 = 5.0 \times 10^{-4}$  J/kg ( $Re_\lambda = 45$ ), integral scale  $\ell = 1.18 \times 10^{-1}$  m and turbulent kinetic energy  $E_1 = 4.8 \times 10^{-2}$  J/kg ( $Re_\lambda = 150$ ), integral scale  $\ell = 1.34 \times 10^{-1}$  m and turbulent kinetic energy  $E_1 = 1.3 \times 10^{-1}$  J/kg ( $Re_\lambda = 250$ ), energy ratio  $E_1/E_2 = 6.7$  for all Reynolds numbers. The initial conditions for the velocity are generated by a linear matching of two homogeneous and isotropic fields over a thickness  $\Delta$ , see Equation (2), while the initial mean scalar distribution is a discontinuity smoothed enough to avoid the Gibbs phenomenon, as in Equation (3).

system is chosen with the  $x$ -axis along the direction of the kinetic energy gradient, axes  $y_1$  and  $y_2$  along the homogeneous directions. The initial condition is obtained by matching two homogeneous and isotropic fields with the same integral scale but each with different turbulent kinetic energy as in [13,14]. In practice, the initial condition is generated as

$$u_i = u_i^{(1)} p(x)^{\frac{1}{2}} + u_i^{(2)} (1 - p(x))^{\frac{1}{2}},$$

135 where  $u_i^{(1)}$  and  $u_i^{(2)}$  are two homogeneous and isotropic velocity fields with turbulent kinetic energies equal to  $E_1$  and  $E_2$ , respectively. The weighting function  $p(x)$ , defined as

$$p(x) = \frac{1}{2} \left[ 1 + \tanh a \frac{x}{L} \tanh a \frac{x - L/2}{L} \tanh a \frac{x - L}{L} \right], \quad (2)$$

has been chosen to allow a smooth transition between the two regions (in Equation 2,  $L$  is the domain size in the  $x$ -direction and  $a$  is a constant, which is chosen in order to have an initial transition layer that is no larger than the integral scale,  $a = 55$ ). The resulting field is then made divergence-free by a standard projection onto a solenoidal space. These operations ensure the continuity of the flow across the whole domain.

140

In this study, we consider the interaction of two flows with the same integral scale and different turbulent kinetic energy, so we choose  $u_i^{(2)} = u_i^{(1)}/\mathcal{E}^{1/2}$ , where  $\mathcal{E} = E_1/E_2$  is the imposed initial kinetic energy ratio.

A description of how the presence of different integral scales can influence the turbulent kinetic energy diffusion can be found in [13,16].

In order to analyse the diffusion of the passive scalar interface across the turbulent kinetic energy gradient, the passive scalar is introduced into the low kinetic energy region of the flow at  $t = 0$ . To avoid the Gibbs phenomenon, the discontinuity is replaced by a sufficiently smooth transition. The initial condition for the passive scalar  $\theta$  is thus defined via the same matching function as

$$\theta(x, y_i) = \frac{1}{2} \left[ 1 - \tanh 2a \frac{x}{L} \tanh 2a \frac{x - L/2}{L} \tanh 2a \frac{x - L}{L} \right]. \quad (3)$$

By choosing  $a = 55$  in Equation (3), the passive scalar interface is smoothed on a length which is about half the initial integral scale. No passive scalar fluctuation is introduced: the passive scalar concentration is initially uniform in the two isotropic regions,  $\theta = 0$  in the high-energy region and  $\theta = 1$  in the low-energy region. Passive scalar variance will be generated by the underlying turbulent flow, see Figure 2.

The mass, momentum, and the passive scalar transport equation are solved by using a dealiased pseudo-spectral Fourier–Galerkin spatial discretisation coupled with a fourth-order Runge–Kutta explicit time integration. The size of the dimensionless computational domain is  $4\pi \times (2\pi)^2$  in the 3D simulations. The domain used in the 2D simulation has the same aspect ratio: it is  $4\pi \times 2\pi$ . For further details on the numerical technique and the initial condition generation, see [13,21,22].

We have carried out a numerical experiment with an imposed initial turbulent kinetic energy ratio of 6.7 in both two and three dimensions. In the 3D simulations, we have performed two experiments in which the higher energy turbulent field  $u_i^{(1)}$  has an initial Taylor microscale Reynolds number equal to 45, 150, and 250.

The domain is discretised with  $256 \times 128^2$  grid points in the simulation at  $\text{Re}_\lambda = 45$ , with  $1200 \times 600^2$  grid points in the simulation at  $\text{Re}_\lambda = 150$  and with  $2048 \times 1024^2$  in the simulation at  $\text{Re}_\lambda = 250$ . The 2D simulations use a  $4096 \times 2048$  grid for an initial integral scale Reynolds number equal to about 3000.

In this first numerical investigation of the passive scalar transport in a shearless energy mixing, the Schmidt number  $\text{Sc} = \kappa/\nu$  is set to 1 in all the simulations. Schmidt numbers of order one are typical of many transport phenomena in air, from small temperature fluctuations to water vapour transport [23].

About 20 initial eddy turnover times have been simulated in two dimensions and 10 initial eddy turnover times in three dimensions. We have estimated that, due to the mixing layer growth, the two separate homogeneous and isotropic regions will be destroyed by their interaction after about 30–35 initial eddy turnover times. Directions  $y_1$  and  $y_2$  in this flow configuration remain statistically homogeneous during the decay, so that all the statistics can be computed as plane averages in these directions. Moreover, in two dimensions, we have enlarged our statistical sample by ensemble averaging also on 50 repetitions of the simulation with different but statistically equivalent initial conditions.

### 3. Passive scalar transport across the interface

The initial conditions for the velocity field produce a kinetic energy gradient in the direction of inhomogeneity ( $x$ ) as already shown in many experiments (e.g. [13,15,24]). Outside

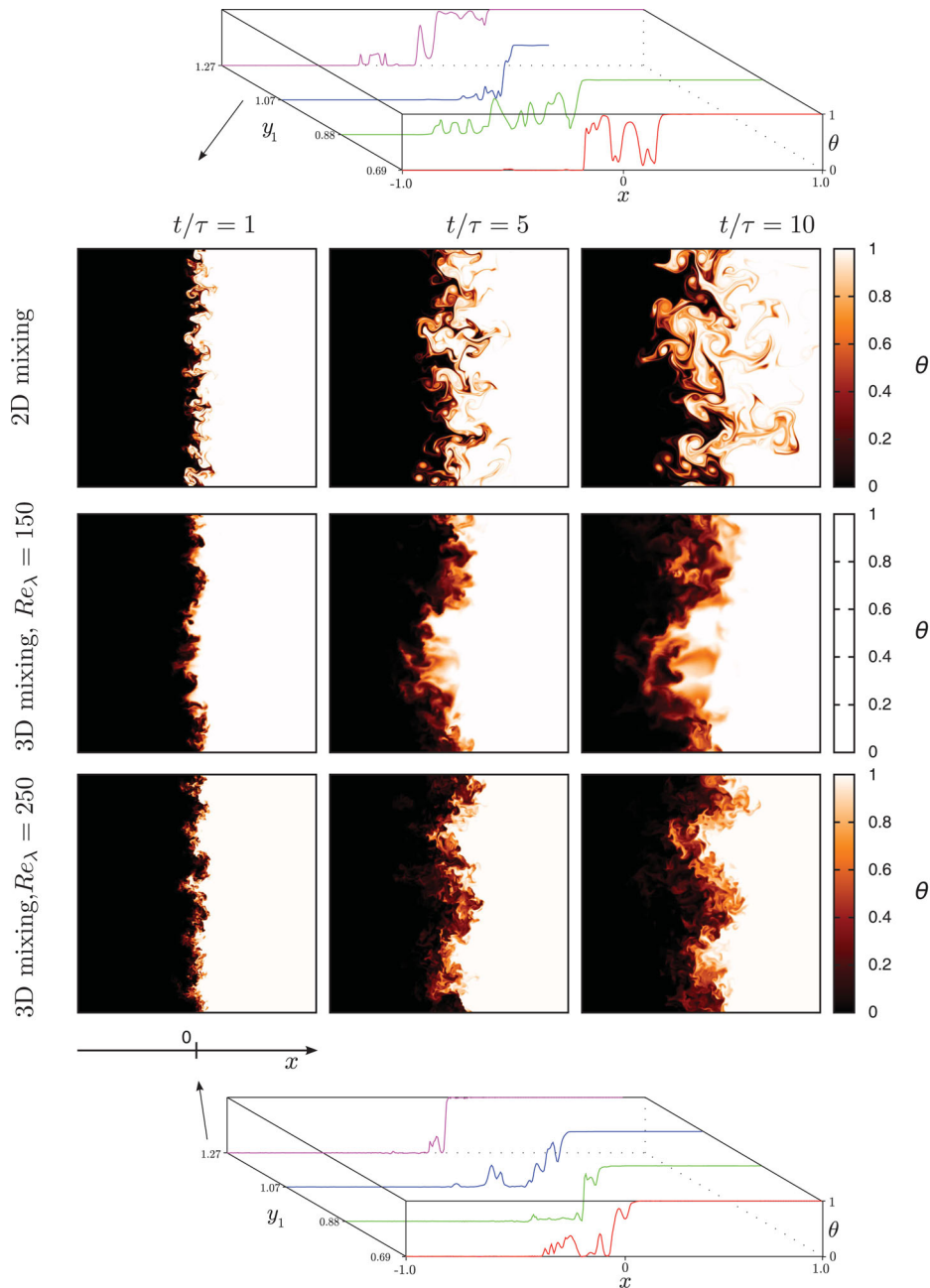


Figure 2. Visualisation of the scalar field in a plane within the central part of the computational domain – the dashed region in Figure 1. The high turbulent energy velocity field is on the left of each image. The three different instants correspond, from left to right, to  $t/\tau = 1, 5, 10$ , respectively.  $\tau$  is the initial eddy turnover time of the high-energy region. The 3D simulation has an initial  $Re_\lambda$  equal to 150 and 250 in the high-energy isotropic region and 60, 100 in the low-energy region. The initial value of the energy ratio of the two interacting isotropic turbulences is 6.7. The insets show the concentration along few lines in the direction parallel to the mean gradient at  $t/\tau = 1$ .



this inhomogeneous region, the kinetic energy shows a power-law decay, with exponents approximately equal to  $-1.2$ , for both  $\text{Re}_\lambda = 150$  and  $\text{Re}_\lambda = 250$  in three dimensions, while no significant energy decay is observed in two dimensions due to the inverse cascade. In both cases, the initially imposed energy ratio between the two homogeneous regions is almost preserved during the time evolution of the flow. 190

In all flow configurations, the velocity mixing layer was observed to be highly intermittent and the velocity fluctuations in the  $x$ -direction have large skewness and kurtosis, see [13,14,24]. Across the mixing layer, the second, the third, and the fourth velocity moments collapse using a single lengthscale; the mixing width  $\Delta_E$ , conventionally defined as the distance between the points with normalised energy  $(E(x, t) - E_2(t))/(E_1(t) - E_2(t))$  195 equal to 0.75 and 0.25. In this paper, we focus on the passive scalar dispersion through the shearless mixing layer. For the velocity statistics, refer to [13,14,24].

As it has been already observed, one-point statistics of the velocity fluctuations along the inhomogeneous direction indicate the presence of a highly intermittent layer which is shifted with respect to the centre of the mixing region towards the lower energy flow 200 [13,14,24]. This is marked by a single large peak of both the skewness and the kurtosis. The intensity of the intermittency and the penetration of this layer are controlled by the kinetic energy gradient and, when present, by the integral scale gradient. The Reynolds number has a minor effect on the large-scale velocity intermittency but has a major impact on the level of small-scale intermittency [15]. 205

The main results of this work is that, in contrast with the velocity transport case, the scalar field is characterised by the presence of the two intermittent fronts which are located at the sides of the interaction region between the two isotropic fields. These fronts can be identified by the peaks of the spatial distributions of the higher order moments of both the scalar field and its derivatives. These two layers delimit a high scalar variance region 210 which is generated by the temporal smoothing of the initial steep scalar gradient, which we identify as our initial thin interface.

### 3.1. Mean scalar diffusion and mixing growth

A visualisation of the time evolution of the passive scalar concentration at three different instants is shown in Figure 2. The passive scalar interface, which initially separates the 215 low-energy region with passive scalar concentration  $\theta = 1$  (on the right of the figures) from the high-energy region with passive scalar concentration  $\theta = 0$ , is spread by turbulent eddies and a passive scalar mixing region with high variance is generated. In Figure 3, a frame of such a set of visualisation is compared with a laboratory visualisation obtained by Jayesh and Warhaft [19]. Scalar concentration isosurfaces are highly corrugated by the 220 advecting velocity eddies as can be seen in Figure 4, which shows the two isosurfaces where the passive scalar concentration is equal to 0.5 and 0.1. These two surfaces appear to be very similar, no difference in the corrugation structures is visually evident, which seems to indicate a possible self-similarity of the process.

In Figure 2, the insets show the concentration distribution along a direction normal 225 to the interface (but aligned with the mean scalar gradient). In the central part of the distributions, some resemblance can be seen with the features called ramp and cliff, first noticed in the 1970s by Gibson, Antonia, Sreenivasan and others (see the review [3] and, for details, [25–28]). These features are considered due to the presence of large-scale straining motions with the direction of compression approximately aligned with the mean scalar 230 gradient. This situation is also met in the present shearless mixing.

The width of the mixing region can be measured by considering the mean passive scalar distributions (Figure 5). The passive scalar mixing layer thickness  $\Delta_\theta$  is defined, in analogy



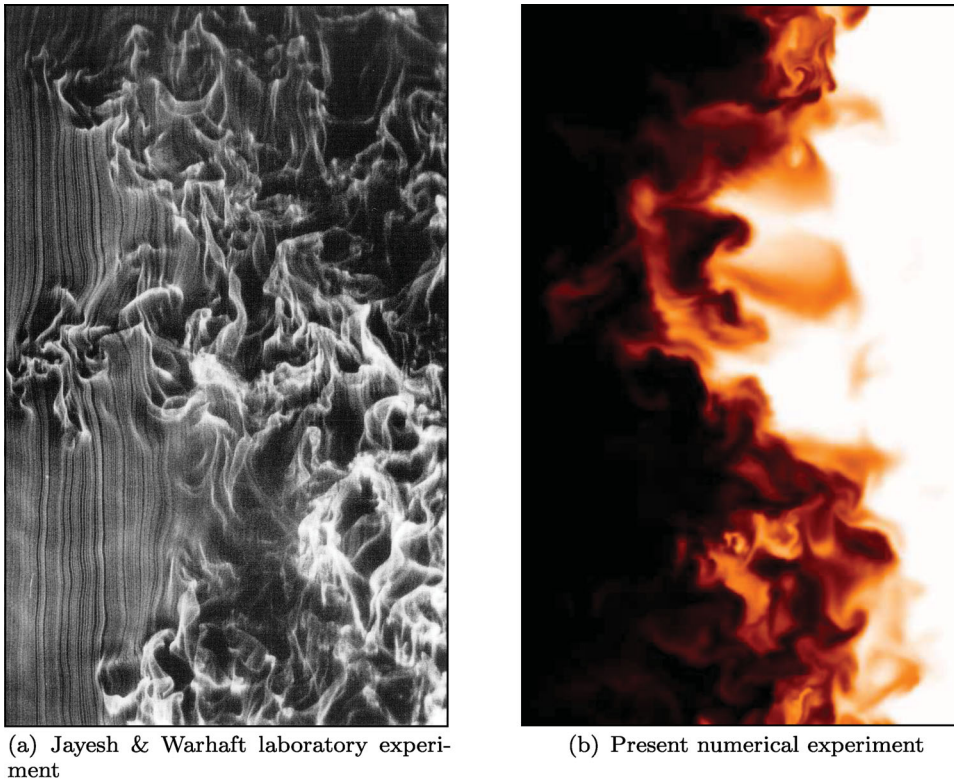


Figure 3. Comparison between a laboratory visualisation by Jayesh and Warhaft ([19] Figure 8(a)) and present simulation: (a) Smoke-wire (streaklines) visualisation of the shearless mixing layer without thermal stratification, wind tunnel experiment, and side view at a distance from the grid equivalent to our time evolution at  $t/\tau \approx 9$ . The flow is from top to bottom and  $Re_\lambda = 130$  [19]. The energy ratio can be estimated as of order  $10^2$  because the turbulence level in the part of the flow out of the grid (on the right in this picture) has a ratio velocity rms/mean velocity less than 0.25%. It should be noted that this visualisation is not exactly the equivalent of the one in panel (b). In fact, the equivalent view would have been a tunnel cross section at a constant  $x$ . (b) Pseudo-colour of the passive scalar concentration along the mixing layer in a central portion of the domain at  $t/\tau = 10$ , initial  $Re_\lambda = 150$ , the initial energy ratio is equal to 6.7.

with the energy layer thickness  $\Delta_E$ , as the distance between the points with mean passive  
 235 scalar  $\bar{\theta}$  equal to 0.75 and 0.25.

After an initial transient of about one eddy-turnover time, the time evolution of these  
 interaction widths follows a trend similar to those observed for the self-diffusion of the  
 velocity field with the same dimensionality, and a stage of evolution with a power law scaling  
 of the scalar mixing thickness is reached in both two and three dimensions. However, the  
 240 time scaling of the growth of the interaction width is superdiffusive in two dimensions  
 ( $\Delta_\theta \sim t^{0.7}$ ), while it is very slightly subdiffusive in three dimensions ( $\Delta_\theta \sim t^{0.46}$  at  $Re_\lambda =$   
 150 and  $\Delta_\theta \sim t^{0.5}$  at  $Re_\lambda = 250$ ) (see Figure 6). Superdiffusive dispersion seems to be  
 a characteristic of 2D flows as observed in [30]. As opposed to 3D turbulence, in two  
 dimensions, vortices tend to live much longer than their turnover time thus enhancing the  
 245 transport.

The same mixing growth can be observed in the absence of the kinetic energy gradient  
 (i.e.  $E_1/E_2 = 1$ ) and thus the mixing width does not seem to be influenced by the presence  
 of the energy gradient.

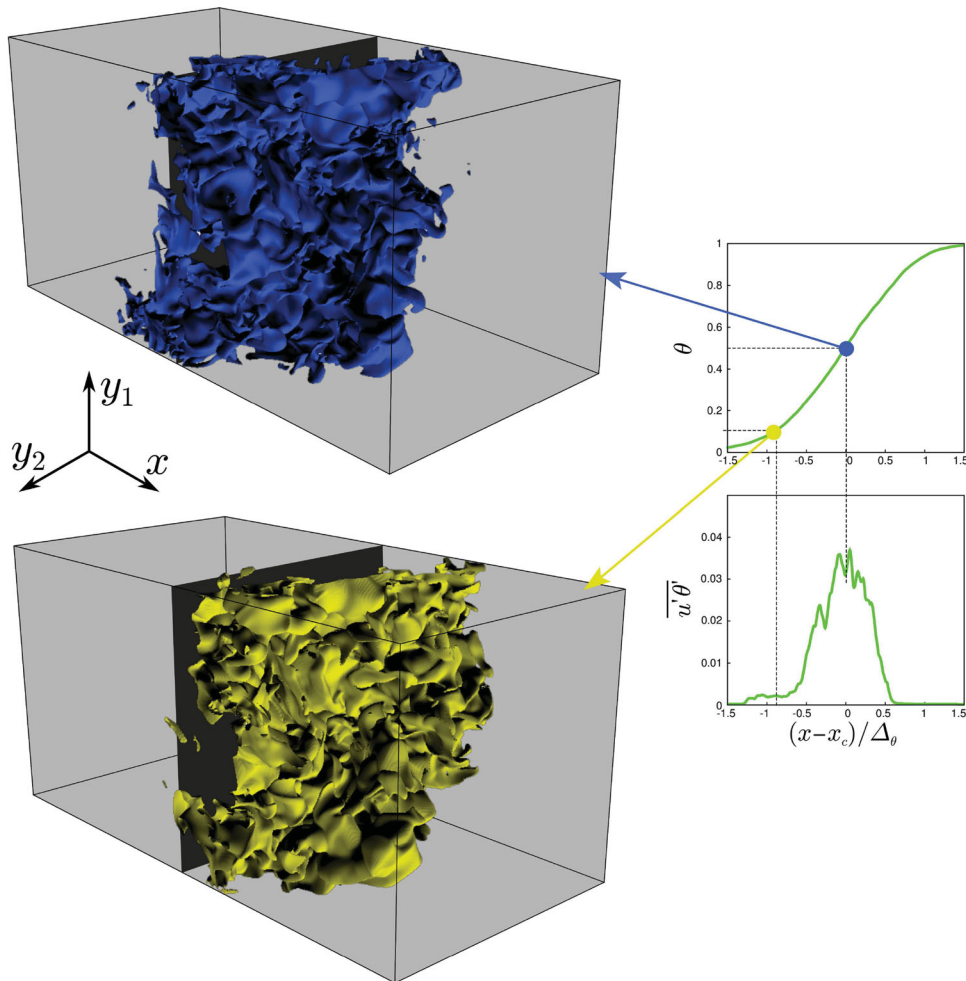


Figure 4. Visualisation of the isosurfaces  $\theta = 0.1$  and  $\theta = 0.5$  of the scalar field at  $t/\tau = 4$ , where  $\tau$  is the initial eddy turnover time of the high-energy turbulence in a portion of the domain – one quarter of each dimension is shown – in the 3D mixing at  $Re_\lambda = 250$ . The low-energy turbulence is on the left of each image, the grey plane in the background is the initial position of the interface.

The 3D simulations also show a fair agreement with the wind tunnel experiments on the scalar diffusion from a line source in a shearless mixing [29]. In particular, the layer thickness grows in almost the same way (see Figure 6), where both sets of data have been plotted, and the scalar flux shows the same asymmetry with respect to the centre of the mixing layer: in both situations, the flux presents lower values on the side where the kinetic energy is lower (see Figure 7(d)–(f)).

### 3.2. Statistics

A mixed region with high passive scalar variance  $\overline{\theta'^2}$ , where  $\theta'$ , defined as

$$\theta'(x, y_i, t) = \theta(x, y_i, t) - \bar{\theta}(x, t),$$

is the fluctuation of the scalar field with respect to its mean value  $\bar{\theta}(x, t)$ , is immediately generated in the centre of the interaction layer. In the 3D flow, the passive scalar variance

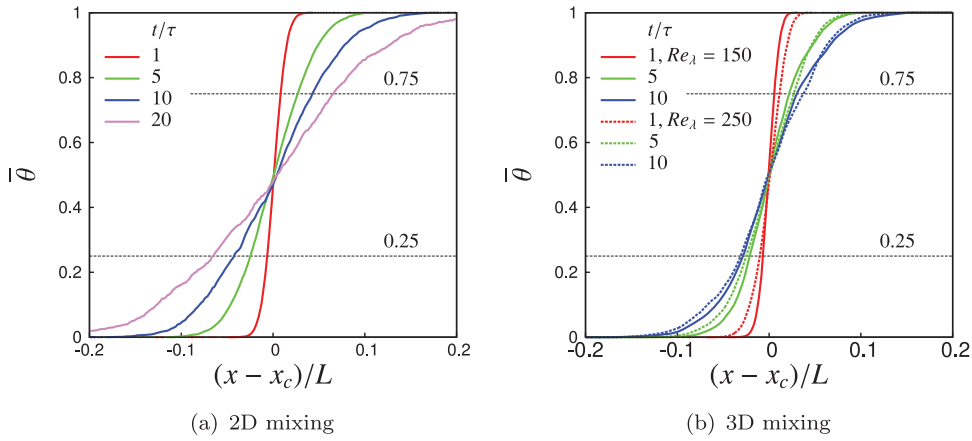


Figure 5. Mean scalar profiles inside the mixing layer: (a) 2D flow, (b) 3D flow. The initial energy ratio  $E_1/E_2$  is equal to 6.7 in both the cases.  $L$  is the domain size in the  $x$ -direction and  $x_c$  the centre of the mixing layer. The dashed horizontal lines indicate  $\bar{\theta} = 0.25$  and  $\bar{\theta} = 0.75$ .

reaches its maximum after less than one eddy turnover time and, after that, it slowly decreases. In the following 10 eddy turnover times, about 20% of the variance present at  $t/\tau = 1$  is lost. In two dimensions, the passive scalar flow is almost twice as large and the initial variance generation lasts longer: the maximum is attained later and is about 50% higher. Notwithstanding the presence of the energy gradient, the mean passive scalar and passive scalar variance profiles are almost symmetric (see Figures 5 and 7).

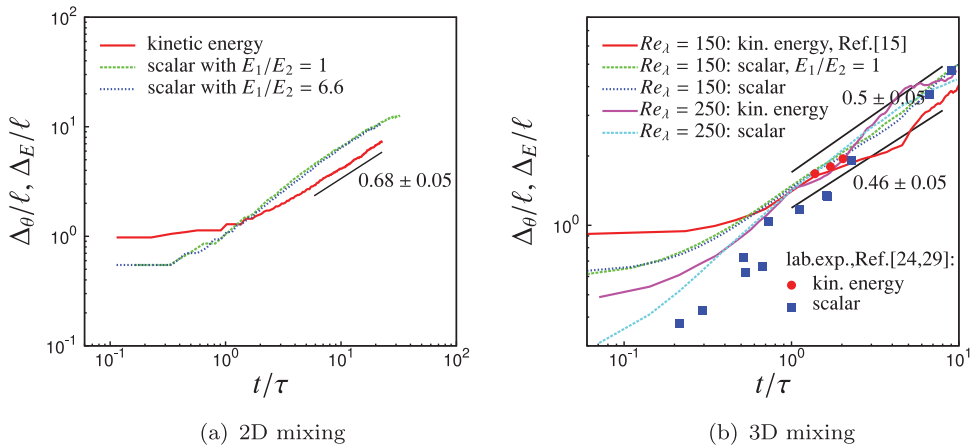


Figure 6. Interaction layer thickness normalised with the initial integral scale  $\ell$ . The scalar layer thickness  $\Delta_\theta$  is defined as the distance between the points where  $\bar{\theta}$  is equal to 0.25 and 0.75. The energy layer thickness is defined as the distance between the points where the normalised turbulent kinetic energy  $(E - E_2)/(E_1 - E_2)$  is equal to 0.25 and 0.75 as in [14,15]. The exponents of the power-law fitting of the scalar thickness growth are indicated. The accuracy of the exponents is about 10%. The same mixing length growth can be observed in the absence of the kinetic energy gradient ( $E_1/E_2 = 1$ ). Experimental data are from the wind tunnel experiments by [24] and [29] with  $E_1/E_2 = 7$ . It should be noted that in this last work the authors propose an exponent of 0.34 for the final stage of the scalar dispersion.

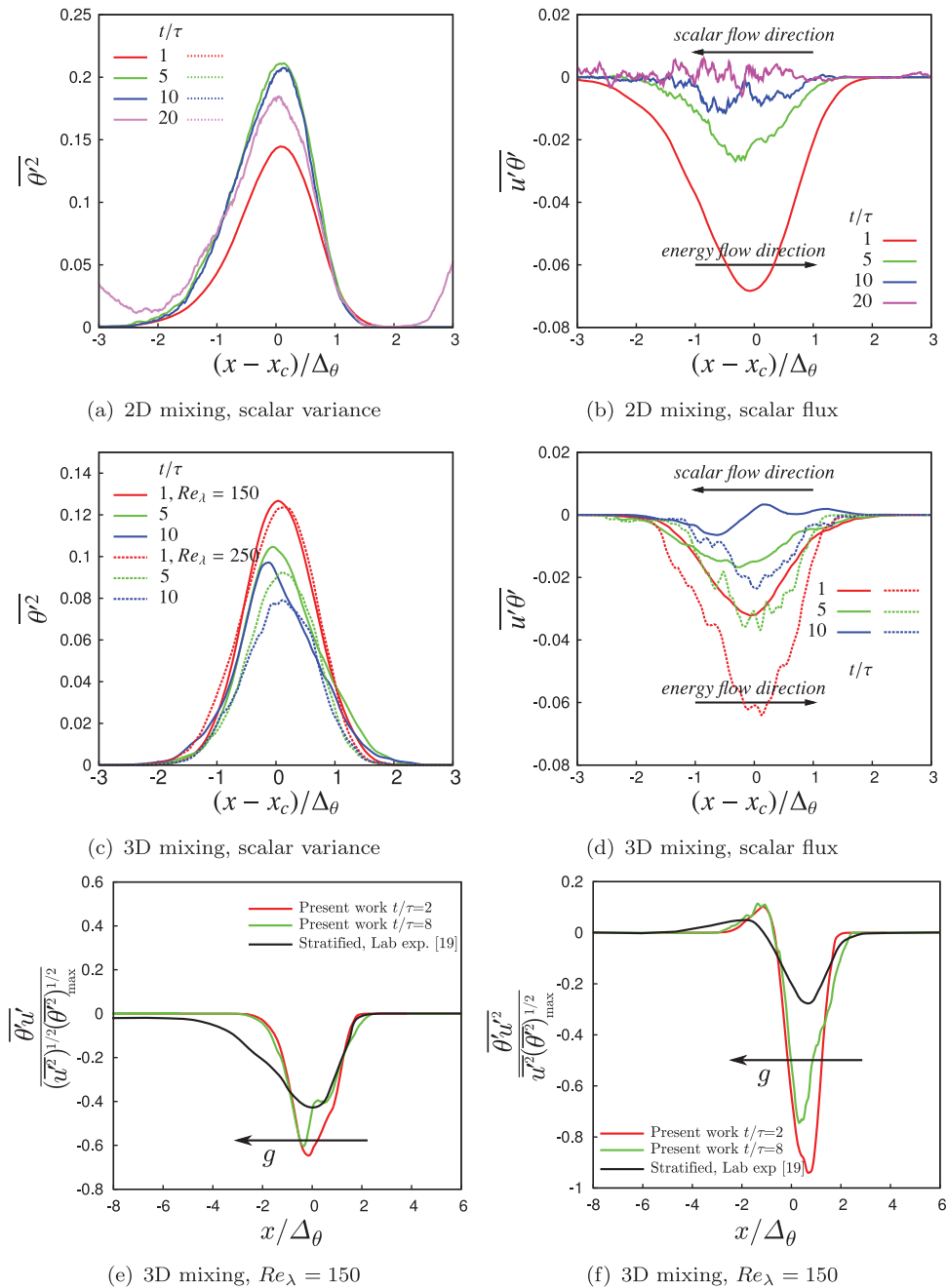


Figure 7. (a,c) Scalar variance in the simulations in two and three dimensions. (b,d) Scalar flux  $u'\theta'$  in the simulations in two and three dimensions. The arrows indicate the scalar and energy flow directions. The initial energy ratio is  $E_1/E_2 = 6.7$  in all simulations;  $\Delta_\theta$  is the passive scalar mixing thickness which increases in time as shown in Figure 6. According to our estimate, for the three dimensions,  $\Delta_\theta \sim t^{0.5}$  at  $Re_\lambda = 250$ , (e) scalar flux, and (f) third-order mixed moment: comparison between the present simulation with an initial Reynolds number  $Re_\lambda = 150$  and laboratory data by [19] at  $Re_\lambda = 130$  obtained in a shearless mixing in the presence of a mild stable temperature stratification (the direction of the gravitational acceleration is indicated by the arrow). In the considered measurement stations,  $x/M = 32$  and the Richardson number is equal to 0.77.

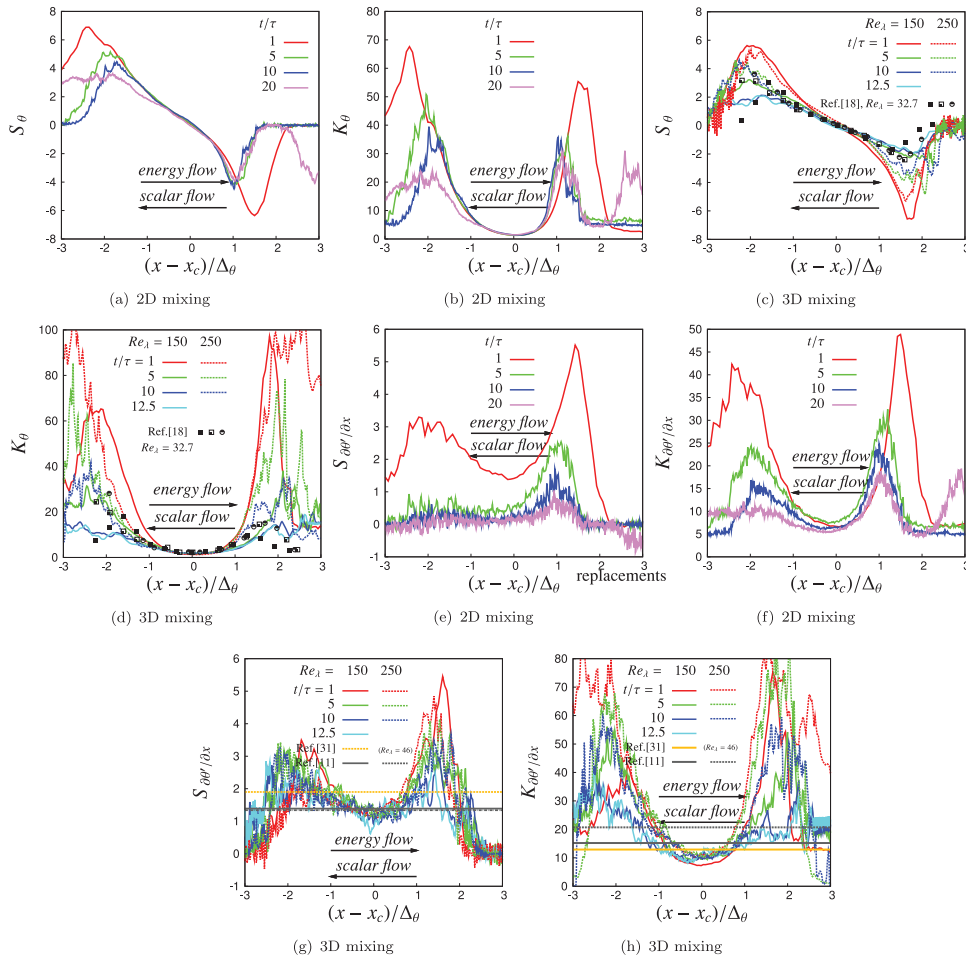


Figure 8. (a,c) Passive scalar skewness distribution and (b,d) passive scalar kurtosis distributions. (e,f) Skewness and (g,h) kurtosis distributions of the derivative of the passive scalar fluctuation in the inhomogeneous direction  $x$ . All the simulations have an initial energy ratio  $E_1/E_2 = 6.7$ . The vertical dashed lines indicate the position of the maximum of intermittence at the end of the simulation. The arrows indicate the passive scalar and energy flow directions which are opposite in these simulations. Leaving aside the sign, the distributions remain unchanged when the passive scalar mean gradient is concurrent with the energy gradient. Symbols in parts (e) and (f) are from the thermal mixing in grid experiments by [18] at  $Re_\lambda = 32.7$ :  $\blacksquare$  mandoline heater,  $x/M = 62.4$ ,  $\square$  toaster heater,  $x/M = 62.4$ ,  $\bullet$  toaster heater,  $x/M = 82.4$ . The Taylor microscale of the homogeneous flow comparison data in parts (g,h) is equal to 140 and 240 in the data by [11] and to 46 in the data by [31].

265 The presence of the turbulent energy gradient is instead felt on the distribution of higher  
 order moments as the passive scalar skewness and kurtosis show in Figure 8 and as the  
 scalar flux shows in Figure 7.

270 In the central region, the values of skewness and kurtosis are closer to the Gaussian  
 ones, while on the mixing edges two peaks can be seen at a distance from the centre  
 approximately equal to  $2\Delta_\theta$ . This means that, in contrast with the velocity field which has  
 a single intermittent layer localised laterally with respect to the centre of the mixing to the  
 region of low energy ( $x/\Delta_E \sim 0.5$  with a kinetic energy ratio equal to 6.7, see also [13,14]),

the third- and fourth-order moments indicate the presence of two intermittent fronts at the border of the mixing region (see Figure 8, panels (a)–(h)). It is interesting to observe that the positions of such peaks, normalised by the scalar mixing layer thickness  $\Delta_\theta$ , seem to collapse, an indication of a possible self-similar regime. This behaviour is observed at all the  $Re_\lambda$  we have simulated and is consistent with the data by Ma and Warhaft [18] in a homogeneous flow at a much lower Reynolds number ( $Re_\lambda \approx 30$ ) (see Figure 8, panels (c)–(d)).

These intermittent fronts are associated with the presence of inhomogeneity in the scalar field, in particular, they are located at a distance from the mixing centre at which the scalar gradient quickly changes. We show, in Section 3.3, that such behaviour is related to the deformation of the initially flat interface in crests and troughs, as shown in Figures 2 and 11. The main effect of the presence of the energy gradient is to make the positions of the two scalar intermittency peaks asymmetric with respect to the centre of the mixing layer, retarding the penetration of the front moving towards the lower energy region.

In the first eddy turnover times, the intermittency at the edges of the mixing layer is very intense, and then decreases as the system evolves: the thickening of the mixing layer and the decay of the kinetic energy reduce the inhomogeneity of the velocity and scalar fields. As a consequence, not only the intermittency levels are reduced, but also the scalar flow tends to disappear (see Figure 7, panels (b)–(d)). In three dimensions, because of the faster energy decay, the intermittency reduction is evident, above all when the  $Re_\lambda = 150$ . In this case, the peaks in the distributions of skewness and kurtosis present the same levels in two and three dimensions after about 1 eddy turnover time but, after 10 eddy turnover times, in two dimensions, the peaks of skewness and kurtosis are twice as high.

The asymmetry observed by Ma and Warhaft [18] in the profiles of skewness and kurtosis is much higher due to the presence of scalar fluctuations in the higher concentration region. These fluctuations are generated by the heater which creates the temperature step. On the contrary, the asymmetries we observe in the first few eddy turnover times are correlated with the presence of a kinetic energy gradient. A second effect present in two dimensions is the different depth of penetration: after about five initial eddy turnover times, the depth of penetration is about  $2\Delta_\theta$  in the high-energy region and about  $\Delta_\theta$  in the low-energy region.

Intermittency is not limited to large-scale passive scalar fluctuations, but is quickly spread to small-scale fluctuations, as can be inferred from the skewness and kurtosis of the passive scalar derivative in the inhomogeneous direction  $x$ , which are shown in Figure 8(e)–(h). Two peaks of large intermittency can be seen in correspondence of the two intermittent fronts since  $t/\tau = 1$ . However, their time evolution is different from the one seen for large-scale passive scalar fluctuations: the peaks always decay in time, but now small-scale intermittency lasts longer in the 3D case. Because the inverse cascade dramatically removes energy from the small scales, in two dimensions the peak of the derivative skewness in the front facing the high-energy region has almost vanished after 10 eddy turnover times while in the front facing the low-energy side it is about half the one present in three dimensions.

The transient scalar derivative moment levels obtained in the two fronts are much higher than the ones observed in isotropic turbulence with a uniform mean scalar gradient at similar Reynolds numbers. For example, Donzis and Yeung [11], in their numerical simulations, obtained a scalar skewness equal to 1.39 at  $Re_\lambda = 140$  and 1.34 at  $Re_\lambda = 240$  with a normalised mean scalar gradient equal to 1. In our experiment, where also the initial mean scalar gradient across the interface was set equal to 1, between  $t = 1\tau$  and  $t = 5\tau$ , we observe a skewness which is in the range of 4–5.5 at  $Re_\lambda = 250$  and between 3 and 5.7 at  $Re_\lambda = 150$ . An even greater departure can be observed in the derivative kurtosis,



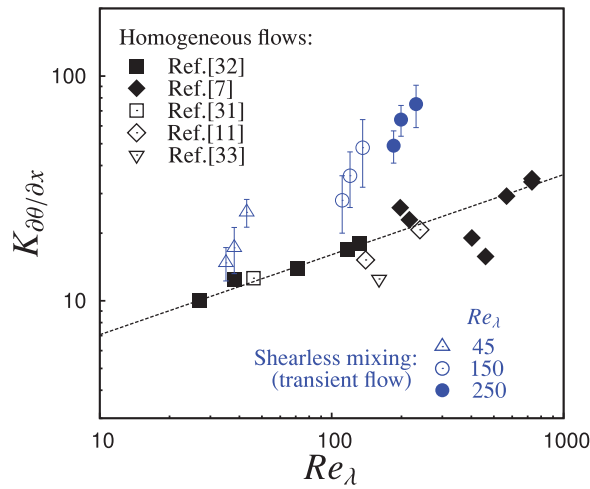


Figure 9. Kurtosis of the scalar derivative as a function of  $Re_\lambda$ . The blue symbols represent the maximum of the kurtosis in the intermittent fronts at  $t/\tau = 1, 5, \text{ and } 10$ ; the black symbols are data for homogeneous flows by Tong and Warhaft [32], Mydlarski and Warhaft [7], Brethouwer *et al.* [31], Donzis and Yeung [11], and Antonia *et al.* [33].

whose extreme values can be twice the values in homogeneous turbulence as shown in Figure 9, where our data are compared with the set of data with derivative parallel to the mean gradient which are included in Figure 3 in the review by Warhaft [3], as well as in [11,31,33] (see also Table 1).

In a laboratory experiment of a decaying grid turbulence with a uniform scalar gradient at  $Re_\lambda = 580$ , Warhaft [3] and Mydlarski and Warhaft [7] found a passive scalar derivative kurtosis close to 20 in the presence of a mean passive scalar gradient equal to about 3.6 K/m (temperature field) after about one eddy turnover time.

The difference becomes more marked as the Reynolds number increases. The intermittency of the two fronts is enhanced by a Reynolds number increment in a way similar to the linear dependence of the intermittency of temperature fluctuations as a function of the Reynolds number observed in a Rayleigh–Bernard convection [34]. This could be a general property of scalar transport. Schumacher observed that the probability density function of the magnitude of the passive scalar gradient increases with the Reynolds number in numerical simulations at moderate Reynolds number [35]. A higher Reynolds number enables

Table 1. Passive scalar gradient and instantaneous Reynolds number for all the simulations:  $Re_\lambda = u'\lambda/\nu$  and  $Re_\ell = u'\ell/\nu$ , where  $\lambda$  is the Taylor microscale and  $\ell$  the integral scale.

	3D mixing						2D mixing	
	Run $Re_\lambda = 45$		Run $Re_\lambda = 150$		Run $Re_\lambda = 250$		2048 × 4096	
Grid	128 <sup>2</sup> × 256		600 <sup>2</sup> × 1200		1024 <sup>2</sup> × 2048		2048 × 4096	
$t/\tau$	$Re_\lambda$	$\nabla\theta$ (m <sup>-1</sup> )	$Re_\lambda$	$\nabla\theta$ (m <sup>-1</sup> )	$Re_\lambda$	$\nabla\theta$ (m <sup>-1</sup> )	$Re_\ell$	$\nabla\theta$ (m <sup>-1</sup> )
0	45	7.51	150	7.65	250	8.49	3076	13.50
1	40	3.11	136	3.12	231	2.85	4762	4.44
5	34	1.20	120	1.32	199	1.25	10200	1.21
10	32	0.80	110	0.92	185	0.89	16297	0.71



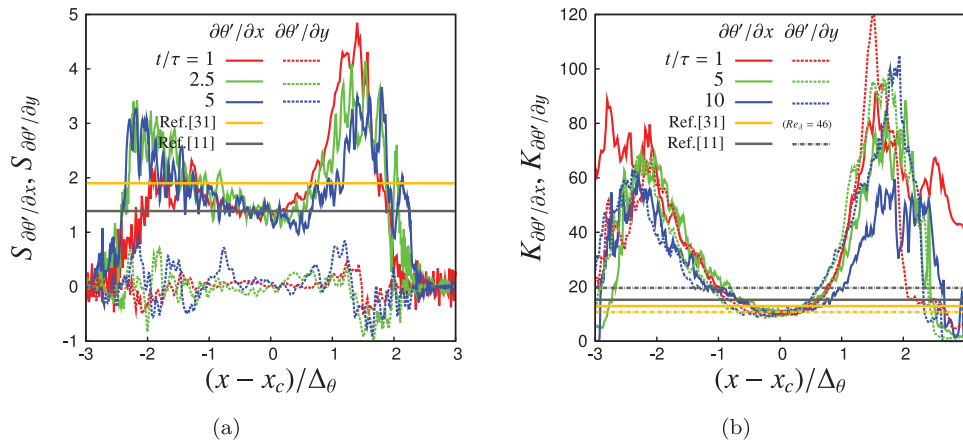


Figure 10. Comparison between the skewness (a) and kurtosis (b) of the passive scalar derivatives  $\partial\theta/\partial x$  and  $\partial\theta/\partial y_1$  in the directions parallel and normal to the energy gradient in the 3D mixing at  $Re_\lambda = 250$ . All present simulations have an initial energy ratio  $E_1/E_2 = 6.7$ . The homogeneous flow data by Donzis and Yeung [11] have a Taylor microscale Reynolds number equal to 240, the data by Brethouwer *et al.* [31] have a Taylor microscale Reynolds number equal to 46.

the passive scalar to be more efficiently stirred on all scales leading to an increase of scalar fluctuations and derivative moments.

Simulations in the absence of a turbulent energy gradient (i.e.  $E_1/E_2 = 1$ ), not shown in the figures, do not show the asymmetry in the position of the scalar intermittent fronts 340 even if the thickness of the mixing layer follows the same temporal growth.

The passive scalar derivative in the directions normal to the kinetic energy and passive scalar gradients (directions parallel to the mixing) shows a slightly reduced level of intermittency in the two fronts but a much reduced asymmetry in its probability density function as its skewness is lower as shown in Figure 10. That is, the passive scalar derivative in the homogeneous direction normal to the mixing process is much less affected by the energy and passive scalar gradients. The Reynolds number and the energy gradient both influence the passive scalar intermittency at small scales [3]. 345

For what concerns the velocity intermittency, as said above, the position of the peak is about at  $x/\Delta_E \sim 0.5$ . The velocity derivative peak is located at  $x/\Delta_E \sim 0.6$  (see reference [15]). Both are slightly shifted toward the lower kinetic energy region with respect to the centre of the mixing. On the contrary, the two peaks of the skewness and kurtosis of the scalar concentration and of its derivative are located at  $x/\Delta_\theta \sim +1.8$  and  $-2.2$ , which correspond to the borders of the high scalar variance region (see Figure 7). Both positions move in time according to the growth of the mixing layer thickness, therefore, the location of the passive scalar intermittency peaks,  $x_{S_\theta}$ , are about three times more distant from the mixing centre with respect to the location of the peak of the velocity intermittency,  $x_{S_u}$ , for the whole flow evolution ( $x_{S_\theta}/x_{S_u} \sim 3$ ). As far as we can see, the positions of the scalar intermittency peaks do not highly depend on the Reynolds number. The main effect of the presence of the energy gradient is to make the positions of the two scalar intermittency peaks asymmetric with respect to the centre of the mixing layer, retarding the penetration of the front moving towards the lower energy region. 350 360

### 3.3. Intermittency generated by linear wave perturbations of the interface

Is the generation of a double intermittency layer specific to a turbulent velocity transport?

365 To answer this question, we have considered a simple 2D situation where the deformation of the interface, represented by the Heaviside function, is due by a single wave with given wave number and frequency. In doing so, the effects of multiple interacting scales on the scalar transport and interface modification will be disregarded. We considered simple velocity waves,

$$u_i = u_0 \sin(kx_j - \omega t), \quad (4)$$

370 and verified that only the velocity normal to the interface and oscillating in space along a direction parallel to the interface produced an undulating interface.

With reference to the system configuration in [Figure 11](#), the perturbation effective in undulating the initially planar scalar interface is  $u = u_0 \sin(ky - \omega t)$ .

375 At the beginning of the process, we assume that the molecular diffusion is negligible in the direction parallel to the interface, i.e.  $\partial^2 \vartheta / \partial y^2$  can be neglected with respect to  $\partial^2 \vartheta / \partial x^2$ . It can then be shown that Equation (1) has the analytical solution,

$$\vartheta(x, y, t) = \frac{1}{2} \left( 1 + \operatorname{erf} \left( \frac{x - \int_0^t u(y, t') dt'}{\sqrt{2\kappa t}} \right) \right), \quad (5)$$

where  $\kappa = Sc \nu$  is the scalar diffusivity. In [Figure 11](#), two visualisations of the scalar concentration field from an initially flat interface can be seen. The scalar fields are obtained from two numerical simulations, the first one (panel (b)) where the velocity field is just  $u =$   
380  $u_0 \sin(ky - \omega t)$  and the second one (panel (c)) where a second wave  $v = v_0 \sin(kx - \omega t)$  is added. This second wave becomes effective in modifying the interface since the instant where the projection of the interface profile along the  $x$ -direction is no more negligible.

In the absence of diffusion, the advection of an interface by a wave like the one represented in [Figure 11](#) panel (b) leads to the black/white configuration where, at any given distance  $x$  from the initial position of the interface, the fraction of space where  $\vartheta = 1$  (flow from right) is  $p(x)$  and the fraction of space where  $\vartheta = 0$  (flow from left) is  $1 - p(x)$ . In this situation, the mean scalar concentration is  $\bar{\vartheta} = p$  and the scalar moments can be easily computed as  $\bar{\vartheta}^n = p(1 - p)[(1 - p)^{n-1} - (-p)^{n-1}]$ . The scalar variance is maximum in the centre and the modulus of all normalised moments increases with  
390 the distance from the centre. In the presence of diffusion, the situation is as depicted in [Figure 11](#) for the simple shear wave represented in panel (b). Diffusion smooths out the interface discontinuity and reduces large deviations from the mean value, thus limiting the maximum skewness and kurtosis. This effect is much more visible at higher wave numbers which have a lower effective Reynolds number.

395 One could expect that the cumulative effect of many basic eddy patterns with different scales (wave numbers) could lead to a fractal corrugation of the surface with higher intermittency. As shown in [\[36\]](#) for 2D turbulence, the distribution of the isoscalar contour length has been found to be fractal at scales larger than the pumping but soon becomes smooth at smaller scale. We think that even such a simple linear model may provide a  
400 generic kinematic picture of the scalar interface and of the formation of a double layer where high moments of the scalar oscillation peak. Holzer and Siggia [\[10\]](#) simulated the mixing of a scalar with an imposed mean gradient in an isotropic turbulent-like flow field and observed that the scalar field has a ramp-cliff structure, i.e. regions of well-mixed

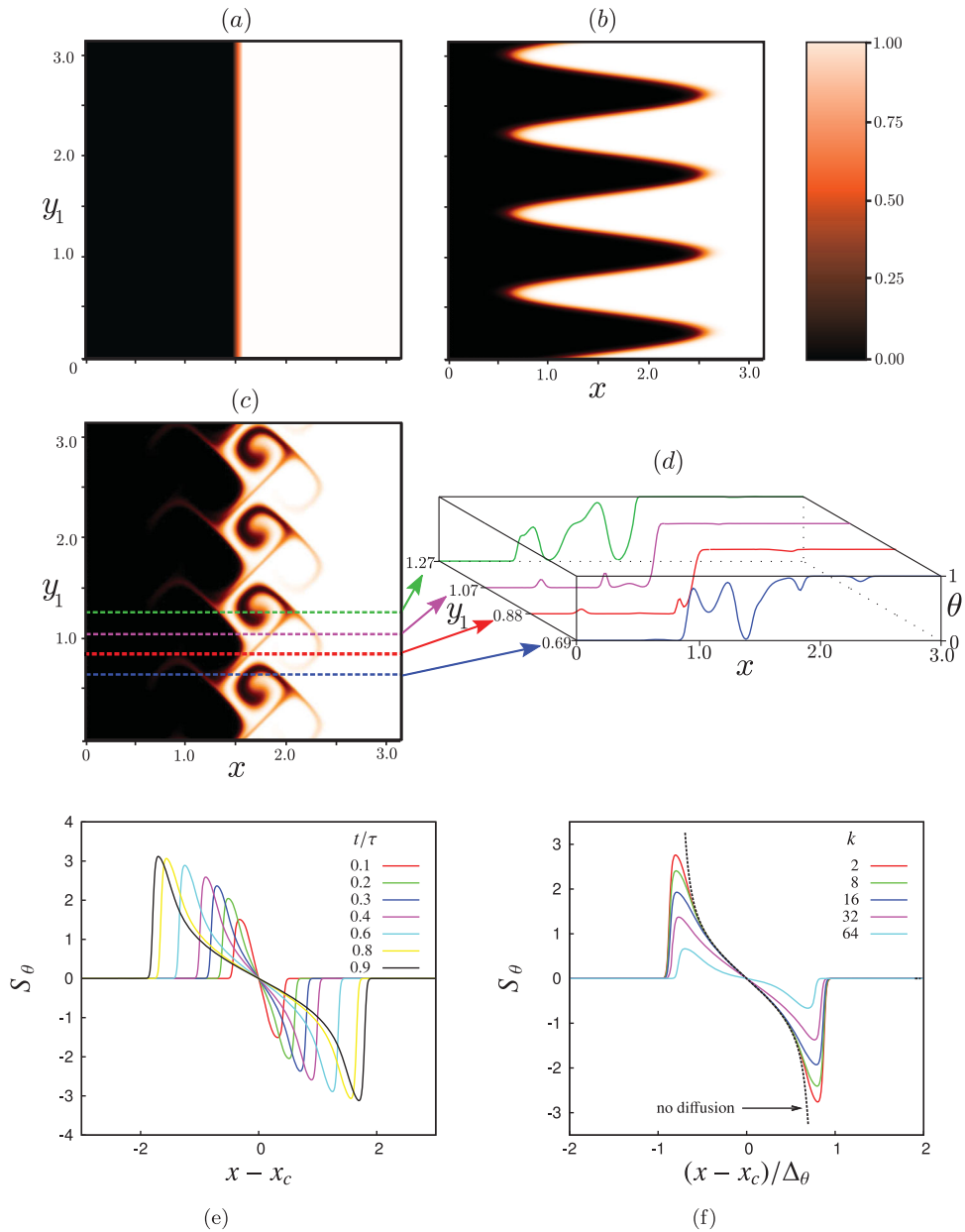


Figure 11. Scalar advection by a wave perturbation: (a) initial scalar concentration; (b) scalar concentration obtained at  $t/\tau = 1$  with the flow field given by Equation (4); (c) scalar concentration at  $t/\tau = 1$  with  $u = u_0 \sin(ky - \omega t)$  and  $v = u_0 \sin(kx - \omega t)$  ( $k = 8$ ,  $u_0 = 1$ ),  $k = 2$ ,  $\text{Re} = u_0(2\pi/k)/\nu = 1420$ ; (d) 1D sections showing the concentration cliffs; (e)–(f) skewness obtained from the simple wave model: (e) time evolution for a shear wave with wave number  $k = 2$  ( $\text{Re} = 5654$ ), (f) data at  $t/\tau = 0.5$  for different wave numbers.

fluid with a nearly constant scalar concentration bounded by steep cliffs. The ramp-cliff structures are positioned approximately perpendicular to the mean gradient and the visualisations suggest that the cliffs are generated by large-scale straining motions with the direction of compression approximately aligned with the mean scalar gradient. In panel (d) of Figure 11, one can see that even in this extremely simplified situation a shadow of ramp-cliff behaviour appears.

#### 410 3.4. *Passive scalar spectra across the mixing layer*

In this last section, we describe briefly the spectral behaviour of the 2D and 3D passive scalar transports across the interface between the two isotropic turbulent fields. This is in comparison with the velocity field. In three dimension, the velocity field undergoes an intense energy cascade. However, in this study we consider turbulence mixing in temporal decay. This circumstance is complex because the forward cascade in temporal decay is concomitant with the small-scale disappearance due to dissipation. In 10 time scales, we observe in this set of simulations, the turbulent energy decays more than the 90% ( $dE/dt \sim t^{-1.2}$ ) [37]. The inertial range is reduced in width (see Figure 12). In two dimensions, the dynamics are more complex as the inverse energy cascade is accompanied by the forward enstrophy cascade. In 10 time scales, the total energy decay is still mild: 14% for a global Reynolds number of about 3000 ( $2048 \times 4096$  resolution). We are thus observing the early part of the transient decay.

The situation is as follows: after a few eddy turnover times, in the central part of the mixing layer, between the two intermittent fronts, the passive scalar fluctuations tend to a slow-varying state. As shown in Figure 7(a) and 7(c), the variance in the centre of the mixing region decays very slowly even in the 3D flow, which has a fast kinetic energy decay of the underlying flow (see [14]). In Figure 12, compensated one-dimensional (1D) passive scalar spectra in the centre of the mixing layer are shown. They show a full range of scales just after one eddy turnover time. The spectra in Figure 12 have been compensated by their inertial range exponents. In the three dimensions, the inertial range scaling  $k^{-5/3}$  has been used [38]. The inertial range seems to be wider for the passive scalar fluctuations than for the velocity fluctuations, a feature already observed [7,39]. In two dimensions, the passive scalar exponent in the inertial range at the end of the transient is about  $-1.7$ , which is roughly one-half of the  $-3$  exponent of the velocity field and is far from the  $k^{-1}$  inertial range scaling of homogeneous and statistically stationary flows (see e.g. [40–42]). In three dimensions, the difference between passive scalar and velocity exponents is very mild and both tend to approach the homogeneous turbulence scaling. However, the passive scalar spectrum seems to show a wider inertial range region, a feature which has been observed also in homogeneous flows at moderate Reynolds numbers (see [7,43]).

We observe that for the present 3D fields, the inertial range scaling exponent for the velocity field is lower than the one of the passive scalar fields as previously noted in [3,43,44]. In particular, in homogeneous isotropic turbulence at  $Re_\lambda = 250$ , Danaila and Antonia [43] found inertial range exponents equal to 1.58 and 1.62 for velocity and passive scalar fields, respectively. In the present 3D numerical experiment, the centre of the mixing layer is characterised by the emerging of an inertial range where the exponents can be estimated as 1.5 (for the velocity field) and 1.62 (for the passive scalar field) at  $Re_\lambda = 250$ . Following Danaila and Antonia [43] and Lee *et al.* [39], we have tried to obtain a relation between the spectral exponent of the scalar and velocity fields. With comparison with the estimations by these authors,  $m_\theta = 5/6 + m_u/2$ , where  $m$  is the modulus of the spectral exponents, we found out that  $m_\theta = 0.57 + 0.67m_u$ . The constant accuracy is  $0.57 \pm 0.11$  and  $0.67 \pm 0.07$ .

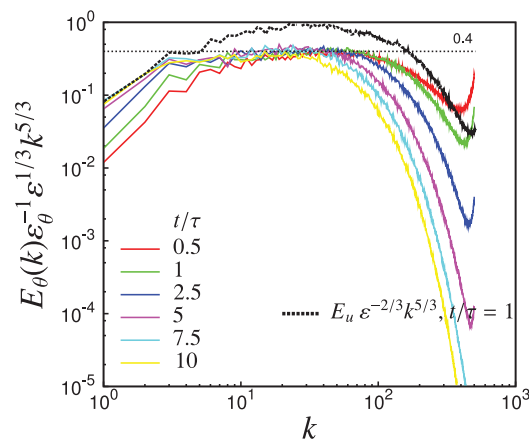
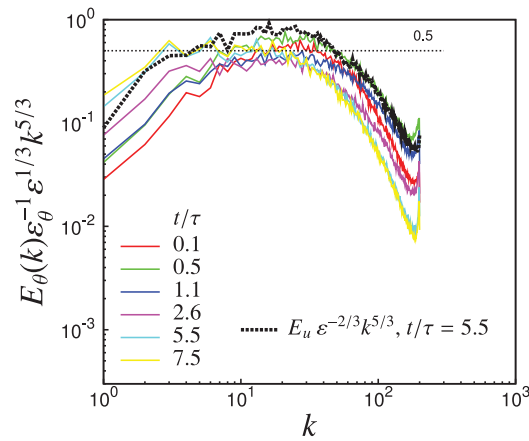
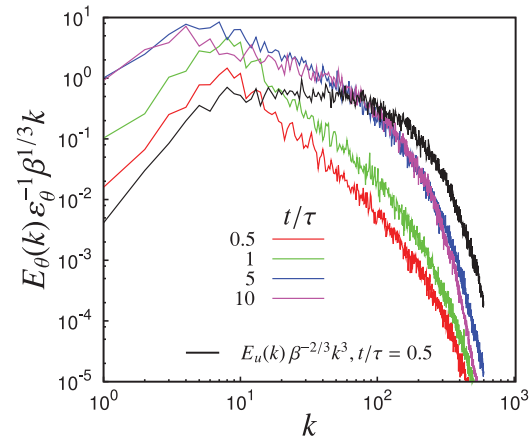
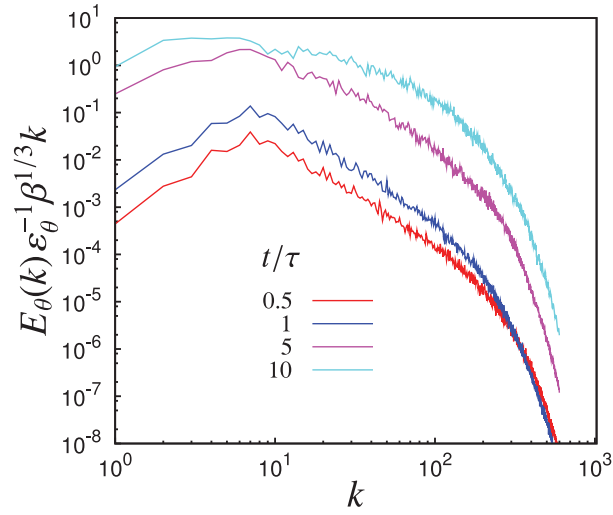
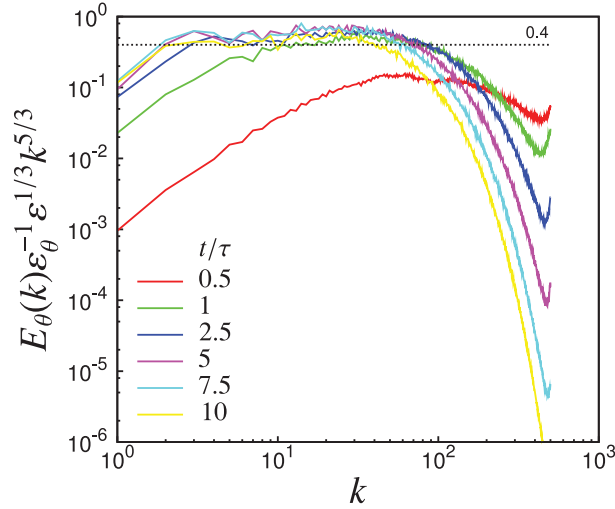


Figure 12. Compensated passive scalar 1D spectra in the centre of the mixing layer in two (part a) and three dimensions (parts b and c). The black dashed lines reproduce, at one instant, the compensated 1D velocity spectrum in the same position.  $\epsilon$  is the dissipation rate,  $\epsilon_\theta$  is the destruction rate of scalar fluctuations, and  $\beta$  is the enstrophy flux. All spectra have been computed by integrating over the homogeneous directions  $y_i$ . All the simulations have an initial energy ratio  $E_1/E_2 = 6.7$ .



(a) 2D mixing



(b) 3D mixing

Figure 13. Compensated passive scalar 1D spectra at a fixed position  $(x - x_c)/\ell(0) = 1.5$  ( $x = x_c + 1.5\ell(0)$ ) in two (a) and three dimensions (b). During the transient, the mixing reaches this position, so that the normalised positions  $(x - x_c)/\Delta_\theta$  are about 1.5, 1.25, 0.5, and 0.25 for  $t/\tau$  equal to 0, 1, 5, 10, respectively, in the 3D mixing at  $\text{Re}_\lambda = 250$ .  $\ell(0)$  is the initial integral scale. All simulations have an initial energy ratio  $E_1/E_2 = 6.7$ .  $\varepsilon$  is the dissipation rate,  $\varepsilon_\theta$  is the destruction rate of scalar fluctuations, and  $\beta$  is the enstrophy flux.

In three dimensions, we found a good agreement with the Kolmogorov–Obukhov–Corrsin scaling. An inertial range with a  $-5/3$  exponent develops. The scaling prefactor  $C_\theta = E_\theta \varepsilon_\theta^{-1} \varepsilon^{1/3} k^{5/3}$ , where  $\varepsilon$  is the dissipation rate and  $\varepsilon_\theta$  is the destruction rate of scalar fluctuations, lies between 0.35 and 0.6, not far from the value of 0.4 which is typical of homogeneous turbulence [45]. The value of  $C_\theta$  is higher in the early stage of the mixing

and tends to slowly reduce as the mixing evolves. A better agreement with this scaling is obtained at higher Reynolds number ( $Re_\lambda = 250$ ) and in the centre of the mixing layer, where the scalar fluctuations are well developed. At the boundary of the mixing region, where the inhomogeneity in both scalar and velocity fields is higher, the scaling constant  $C_\theta$  is higher, i.e. 0.5–0.7. 460

In two dimensions, our data do not show the scaling present in homogeneous flows [40,41]: the scalar spectrum exponent does not remain constant and tends to  $-1.7 \pm 0.2$  after 10 eddy turnover times. This value is different from both the  $-1$  scaling of the inertial–convective range and the  $-5/3$  scaling exponent of the convective–diffusive range. This can be again a consequence of the flow inhomogeneity, that is more influential than in the 3D case. 465

As a general observation, we may say that the spectra of the passive scalar fluctuations seem to have an asymptotic behaviour in the mixing region. As the front moves toward the homogeneous regions, the passive scalar spectra increase and its exponent tends to  $-5/3$  (see Figure 13). This  $-5/3$  regime is anyway in basic agreement with the studies on passive scalar transport in homogeneous flows. For example, it has been found that such regime appears even in homogeneous shear flows for wave numbers higher than the crossover shear wave number [46]. 470

The situation is different for the 2D field, because in this case the spectral exponent inside the transient mixing changes little,  $m_u = -3 \pm 0.2$ . Here the Reynolds effects are not visible. For the scalar field instead, the situation is opposite, the exponent variation is large, from  $m_\theta = -2.7$  at  $t/\tau = 0.5$  to  $m_\theta = -1.7$  at  $t/\tau = 10$ . Once again, the passive scalar field differs substantially from the transport carrier. We have here a situation partly similar to what observed by Bos *et al.* [40], see Figure 4 therein. In the paper, where homogeneous isotropic turbulence forced at small wave numbers is considered (forward enstrophy cascade), the scalar spectrum shows to be substantially smaller than the velocity one ( $-1$  against  $-3$ ). On this respect, we should point out that the inhomogeneity and anisotropy effects may limit the decrease of scalar spectral exponent with respect to the velocity exponent. Furthermore, a priori we do not know the length of the transient. It is possible that we are still inside the early part of the transient where the forward cascade has not had time to settle on the asymptotic state. This aspect needs to be considered more in depth with further dedicated experiments. 475 480 485

#### 4. Conclusions

We have carried out a set on numerical experiments on the transport of a passive scalar through the interfacial layer separating two decaying isotropic turbulent flows with different levels of kinetic energy. This system is a shearless mixing, possibly the simplest inhomogeneous turbulent flow because of the lack of a mean flow and thus no generation of turbulent energy. The system has a high degree of generality, since it is unsteady, inhomogeneous, and anisotropic. 490 495

We have compared the advection of the scalar field in two and three dimensions. The evolution of the passive scalar field has been analysed by means of one-point statistics and spectra computations.

The main conclusions are the following. The diffusion length of the scalar,  $\Delta_\theta$ , follows closely the temporal evolution of the self-diffusion of the velocity field,  $\Delta_E$ . In two dimensions, the growth is faster:  $\Delta_E \sim \Delta_\theta \sim t^{0.68 \pm 0.05}$ , while in three dimensions,  $\Delta_E \sim \Delta_\theta \sim t^{0.48 \pm 0.05}$ . At equal times in the transient, the scalar flow is about twice as large 500



in two dimensions than in three dimensions. Also, the scalar variance in the centre of the mixed layer is 50% higher in two dimensions.

505 An important observation concerns the presence of two scalar intermittent fronts which appear at the sides of the mixed region. The intermittency levels of the fronts are initially high and gradually decay in time. In all simulations, the fronts move away from the initial position of the interface. The front on the high-energy side of the mixing penetrates deeper into it. This asymmetry is milder in the 3D case.

510 The intermittency is not limited to the large scales, but involves also the small scales. In two dimensions, the small-scale intermittency decay is fast. In three dimensions, the decay is slower and the kurtosis values are sensibly higher. The large-scale intermittency is less affected by dimensionality issues, though the kurtosis is higher in three dimensions.

515 To understand the formation of the double intermittent layer, we carried out an analysis based on simple wavy perturbations of the interface. The formation of the bilayer is once again observed and is promoted by undulations which are normal to the interface and propagates along it. Since in this case the flow field is linear and may contain only one spatial and one temporal scales, we may infer that the bilayer formation is a general dynamic characteristic. Thus, it is not specific to the turbulent transport.

520 In the centre of the shear-free mixing layer, in three dimensions, the passive scalar and velocity spectra both show an inertial range with an exponent close to  $-5/3$ . The passive scalar exponent is found to be always a bit larger than the energy exponent, in agreement to previous laboratory experiments in grid turbulence.

525 In two dimensions, the inertial range energy scaling is close to  $k^{-3}$ , while the passive scalar tends to  $k^{-1.7}$ . At the end of the transient evolution in both cases we observed (10 time scales), we found an exponent value which is closer to the 3D  $k^{-5/3}$  forward cascade than to the 2D  $k^{-1}$  Batchelor's scaling. In this regard, in our early/midterm transients, we see two possible sceneries. First, the forward enstrophy cascade is still far from its temporal asymptote. Second, the presence of inhomogeneity and anisotropy can affect the passive scalar spectral exponent with respect to that of the kinetic energy.

### Acknowledgements

535 It is our great pleasure to dedicate this paper to this special journal issue celebrating Professor Robert Antonia's outstanding contributions to fluid dynamics on the occasion of his 70th birthday. We thank Professor Antonia and his scientific work for giving a true inspiration.



We are grateful to Professor Zellman Warhaft of Cornell University who encouraged our study and shared the visualisation in [Figure 3](#). We thank the referees for their constructive reviews and the many suggestions.

### 540 Funding

This work was partially supported by the PRACE partnership (<http://www.prace-ri.eu>) [grant number 2011050773]; CINECA computing centre (<http://www.cineca.it>) [grant number ISCRA HP10ACLN4]. We thank also HPC@POLITO (<http://www.hpc.polito.it>) for the availability of computational resources.

### 545 References

- [1] K.R. Sreenivasan and R.A. Antonia, *The phenomenology of small-scale turbulence*, Ann. Rev. Fluid Mech. 29 (1997), pp. 435–472.
- [2] B.I. Shraiman and B.I. Siggia, *Scalar turbulence*, Nature 405 (2000), pp. 639–646.

- [3] Z. Warhaft, *Passive scalar in turbulent flows*, Ann. Rev. Fluid Mech. 32 (2000), pp. 203–240.
- [4] U. Frisch, *Turbulence: the legacy of A.N. Kolmogorov*, Cambridge University Press, Cambridge, 1995. 550 
- [5] J.C.R. Hunt, J.C. Kaimal, and J.E. Gaynor, *Eddy structure in the convective boundary-layer – new measurements and new concepts*, Q. J. Royal Meteorol. Soc. 114 (1988), pp. 827–858.
- [6] A. Pumir, *A numerical study of the mixing of a passive scalar three dimensions in the presence of a scalar gradient*, Phys. Fluids 6 (1994), pp. 2118–2132. 555
- [7] L. Mydlarski and Z. Warhaft, *Passive scalar statistics in high Peclet number grid turbulence*, J. Fluid Mech. 358 (1998), pp. 135–175.
- [8] R.H. Kraichnan, *Convection of a passive scalar by a quasi-uniform random straining field*, J. Fluid Mech. 64 (1974), pp. 737–762.
- [9] R.H. Kraichnan, *Anomalous scaling of a randomly advected passive scalar*, Phys. Rev. Lett. 72 (1994), pp. 1016–1019. 560
- [10] M. Holzner and E.D. Siggia, *Turbulent mixing of a passive scalar*, Phys. Fluids 6 (1994), pp. 1820–1837.
- [11] D.A. Donzis and P.K. Yeung, *Resolution effects and scaling in numerical simulations of passive scalar mixing in turbulence*, Phys. D 239 (2010), pp. 1287–1287. 565
- [12] L. Danaïla, R.A. Antonia, and P. Burattini, *Comparison between kinetic energy and passive scalar energy transfer in locally homogeneous isotropic turbulence*, Phys. D 241 (2012), pp. 224–231.
- [13] D. Tordella and M. Iovieno, *Numerical experiments on the intermediate asymptotics of the shear-free turbulent transport and diffusion*, J. Fluid Mech. 549 (2006), pp. 429–441. 570
- [14] D. Tordella, M. Iovieno, and P.R. Bailey, *Sufficient condition for Gaussian departure in turbulence*, Phys. Rev. E 77 (2008), 016309.
- [15] D. Tordella and M. Iovieno, *Small scale anisotropy in the turbulent shearless mixings*, Phys. Rev. Lett. 107 (2011), 194501.
- [16] D. Tordella and M. Iovieno, *Decaying turbulence: what happens when the correlation length varies spatially in two adjacent zones*, Phys. D 242 (2012), pp. 270–281. 575
- [17] T. Gotoh, T. Watanabe, and Y. Takeshi, *Universality and anisotropy in passive scalar fluctuations in turbulence with uniform mean gradient*, Phys. D 241 (2012), pp. 141–148.
- [18] B. Ma and Z. Warhaft, *Some aspects of the thermal mixing layer in grid turbulence*, Phys. Fluids 29 (1986), pp. 3114–3120. 580
- [19] Jayesh and Z. Warhaft, *Turbulent penetration of a thermally stratified interfacial layer in a wind-tunnel*, J. Fluid Mech. 277 (1994), pp. 23–54.
- [20] J. Westerweel, C. Fukushima, J. Pedersen, and J.C.R. Hunt, *Momentum and scalar transport at the turbulent/non-turbulent interface of a jet*, J. Fluid Mech. 631 (2009), pp. 199–230.
- [21] M. Iovieno, C. Cavazzoni, and D. Tordella, *A new technique for a parallel dealiased pseudo-spectral Navier-Stokes code*, Comput. Phys. Commun. 141 (2001), pp. 365–374. 585
- [22] D. Tordella, M. Iovieno, and L. Ducasse, *Dimensionality influence on passive scalar transport*, J. Phys. Conf. Ser. 318 (2012), 052042. 
- [23] P. Yeung, D.A. Donzis, and K.R. Sreenivasan, *Simulation of three-dimensional turbulent mixing for Schmidt numbers of order 1000*, Flow Turbul. Combust. 72 (2004), pp. 333–374. 590
- [24] S. Veeravalli and Z. Warhaft, *The shearless turbulence mixing layer*, J. Fluid Mech. 207 (1989), pp. 191–229.
- [25] C.H. Gibson, C.A. Friehe, and S.O. McConnel, *Skewness of temperature derivatives in turbulent shear flows*, Phys. Fluids 20 (1977), pp. 156–167.
- [26] P.G. Mestayer, C.H. Gibson, M.F. Coantic, and A.S. Patel, *Local anisotropy in heated and cooled turbulent boundary layer*, Phys. Fluids 19 (1976), pp. 1665–1673. 595
- [27] K.R. Sreenivasan and R.A. Antonia, *Skewness of temperature derivatives in turbulent shear*, Phys. Fluids 20 (1977), pp. 1989–1988.
- [28] K.R. Sreenivasan, R.A. Antonia, and D. Britz, *Local isotropy and large structures in a heated turbulent jet*, J. Fluid Mech. 94 (1979), pp. 745–775. 600
- [29] S. Veeravalli and Z. Warhaft, *Thermal dispersion from a line source in the shearless turbulence mixing layer*, J. Fluid Mech. 216 (1990), pp. 35–70.
- [30] A.E. Hansen, D. Marteau, and P. Tabeling, *Two-dimensional turbulence and dispersion in a freely decaying system*, Phys. Rev. E 58 (1998), pp. 7261–7271.

- 605 [31] G. Brethouwer, J.C.R. Hunt, and F.T.M. Nieuwstadt, *Micro-structure and Lagrangian statistics of the scalar field with a mean gradient in isotropic turbulence*, J. Fluid Mech. 474 (2003), pp. 193–225.
- [32] C.R. Tong and Z. Warhaft, *On passive scalar derivative statistics in grid turbulence*, Phys. Fluids 6 (1994), pp. 2165–2176.
- 610 [33] R.A. Antonia, F. Anselmet, and A.J. Chambers, *Assessment of local isotropy using measurements in a turbulent plane jet*, J. Fluid Mech. 163 (1986), pp. 365–391.
- [34] M.S. Emran and J. Schumacher, *Fine-scale statistics of temperature and its derivatives in convective turbulence*, J. Fluid Mech. 611 (2008), pp. 13–34.
- [35] J. Schumacher and K.R. Sreenivasan, *Statistics and geometry of passive scalars in turbulence*, Phys. Fluids 17 (2005), pp. 1–19.
- 615 [36] M. Vucelja, G. Falkovich, and K.S. Turitsyn, *Fractals iso-contours of Passive scalar in two-dimensional smooth random flows*, J. Stat. Phys. 147 (2012), pp. 424–435.
- [37] P. Burattini, P. Lavoie, A. Agrawal, L. Djenidi, and R.A. Antonia, *Power law of decaying homogeneous isotropic turbulence at low Reynolds number*, Phys. Rev. E 73 (2006), 066304.
- 620 [38] T. Watanabe and T. Gotoh, *Scalar flux spectrum in isotropic steady turbulence with a uniform mean gradient*, Phys. Fluids 19 (2007), 121707.
- [39] S.K. Lee, A. Benaissa, L. Djenidi, P. Lavoie, and R.A. Antonia, *Scaling range of velocity and passive scalar spectra in grid turbulence*, Phys. Fluids. 24 (2012), 075101.
- [40] W.J. Bos, B. Kadoch, K. Schneider, and J.P. Bertoglio, *Inertial range scaling of the scalar flux spectrum in two-dimensional turbulence*, Phys. Fluids 21 (2009), 115105.
- 625 [41] T. Gotoh, J. Nagaki, and Y. Kaneda, *Passive scalar spectrum in the viscous-convective range in two-dimensional steady turbulence*, Phys. Fluids 12 (2000), pp. 155–168.
- [42] T. Gotoh, T. Watanabe, and Y. Suzuki, *Scalar flux in a uniform mean scalar gradient in homogeneous isotropic steady turbulence*, J. Turbul. 12 (2011), pp. 1–27.
- 630 [43] L. Danaila and R.A. Antonia, *Spectrum of a passive scalar in moderate Reynolds number homogeneous isotropic turbulence*, Phys. Fluids. 21 (2009), 111702.
- [44] T. Zhou, R.A. Antonia, and L.P. Chua, *Performance of a probe for measuring turbulent energy and temperature dissipation rates*, Exp. Fluids 33 (2002), pp. 334–345.
- [45] K. Sreenivasan, *The passive scalar spectrum and the Obukhov–Corrsin constant*, Phys. Fluids 8 (1996), pp. 189–196.
- 635 [46] A. Celani, M. Cencini, M. Vergassola, E. Villermaux, and D. Vincenzi, *Shear effects on passive scalar spectra*, J. Fluid Mech. 823 (2005), pp. 99–108.